Supplemental Information

Effect of heterogeneous oxidative aging on light absorption by biomass-burning organic aerosol

Eleanor C. Browne,[1*] Xiaolu Zhang,[2] Jonathan P. Franklin,[3] Kelsey J. Ridley,[3] Thomas W. Kirchstetter,[4,5] Kevin R. Wilson,[6] Christopher D. Cappa,[7] and Jesse H. Kroll[3]

[1]Department of Chemistry and Cooperative Institute for Research in Environmental Sciences, University of Colorado Boulder, Boulder, Colorado 80309, United States.

[2]Air Quality Research Center, University of California Davis, Davis, California, 95616, United States

[3]Department of Civil and Environmental Engineering, Massachusetts Institute of Technology, Cambridge, Massachusetts 02139, United States

[4]Energy Technologies Area, Lawrence Berkeley National Laboratory, Berkeley, California 94720, United States

[5]Department of Civil and Environmental Engineering, University of California Berkeley, Berkeley, California 94720, United States

[6]Chemical Sciences Division, Lawrence Berkeley National Laboratory, Berkeley, California 94720, United States

[7]Department of Civil and Environmental Engineering, University of California Davis, Davis, California, 95616, United States

*email: eleanor.browne@colorado.edu

Description of Optical Closure Method

Values of the time-evolving effective complex refractive index (CRI = $n + ki$) are calculated for the oxidized smoke particles by simultaneously minimizing the difference between calculated and observed absorption and extinction coefficients. The calculations assume spherical particles with size-independent, homogeneous composition and are performed using spherical particle Mie theory. The observed number-weighted particle size distribution is used as an input for the calculations. The extinction and absorption coefficients (b_{ext} and b_{abs}; units = 1/Mm) are calculated by integrating across the entire size distribution as:

$$b_{abs} = \int_{d_{p,min}}^{d_{p,max}} \sigma_{abs} \cdot \left(\frac{dN}{dlog(d_p)}\right) dlog(d_p)$$

and

$$b_{ext} = \int_{d_{p,min}}^{d_{p,max}} \sigma_{ext} \cdot \left(\frac{dN}{dlog(d_p)}\right) dlog(d_p)$$

where $d_{p,min}$ and $d_{p,max}$ are the minimum and maximum particle diameters, s_{abs} and s_{ext} are the size-dependent absorption and extinction cross-sections (m^2 $particle^{-1}$), respectively, and $dN/d\log(d_p)$ is the number-weighted particle size distribution. The retrieved effective CRI is the value that minimizes the merit function:

$$MF = \frac{\left(b_{ext,obs} - b_{ext,calc}\right)^2}{\epsilon_{ext,meas}^2} + \frac{\left(b_{abs,obs} - b_{abs,calc}\right)^2}{\epsilon_{abs,meas}^2}$$

where $e_{ext,meas}$ and $e_{abs,meas}$ are the estimated measurement uncertainties. For each OH or O_3 exposure, a value of the effective CRI was retrieved for every measured size distribution using the average observed b_{ext} and b_{abs} across the size distribution measurement period; the reported effective CRI values for each OH or O_3 exposure are the average of the retrieved values for each size distribution measurement. In general, the value of *n* is more sensitive to the first term and the value of *k* more sensitive to the second term of the *MF*, although there is some cross-sensitivity and, as shown by (Zarzana, Cappa, and Tolbert 2014), using both extinction and absorption measurements overall provides for tighter constraints on the retrieved value of both *n* and *k*. The assumption of spherical particles is appropriate for particles produced from smoldering biomass combustion, especially low-temperature combustion, and of aged biomass combustion derived particles (Sumlin et al. 2017; Chakrabarty et al. 2010; Martins et al. 1998). The assumption of homogeneous composition is consistent with SEM and TEM images of tar balls produced from smoldering combustion (Sumlin et al. 2017; Pósfai et al. 2004), although we note that tar balls and the organic particles sampled here may not be identical. Absent evidence to the contrary, we assume that the particles have homogeneous composition.

Uncertainties in the retrieved *n* and *k* are determined through a Monte Carlo analysis where the input b_{ext} and b_{abs} and the input size distribution are varied within their respective uncertainty ranges. More specifically, a normal distribution around the observed b_{ext} and b_{abs} is used with a width of ±4% for b_{ext} and ±8% for b_{abs}. A normal distribution of particle concentrations is also used, with a width of ±10%. The uncertainty in the particle diameters is assumed to be log-normally distributed, with an uncertainty of ±log(0.01) for each diameter. A total of 1000 iterations of the retrieval were performed both for 405 nm and 532 nm. The uncertainties in the retrieved *n* and *k* are taken as the 1s width of the resulting distribution of *n* and *k* values. The uncertainty in *n* is ±0.06 at both 405 nm and 532 nm. The uncertainty in *k* is ±0.0005 at 405 nm and ±0.00011 at 532 nm. The smaller uncertainty at 532 nm than at 405 nm is because the percent uncertainty in *k* is approximately conserved and the absolute value of *k* is smaller at 532 nm. There is a slight positive correlation between the retrieved *n* and *k* at a given wavelength.

Experiment	Ozone exposure range (molecules s cm^{-3})	OH exposure range (molecules s cm^{-3})	Total aerosol number (number cm^{-3})	Total aerosol volume ($\mu m\ cm^{-3}$)	Mean surface area weighted diameter (nm)
Ozone	$0 – 4.5 \times 10^{15}$	N/A	4.3×10^{4}	82	135
OH + ozone	$0.32 – 1.8 \times 10^{16}$	$2.65 – 6.75 \times 10^{11}$	1.1×10^{5}	373	155
No oxidation (Fig. S2)	N/A	N/A	4.7×10^{4}	79	139
No oxidation (Fig. S3)	N/A	N/A	1.6×10^{5}	984	192

Table S1 Experimental parameters for the experiments discussed in the manuscript. The aerosol characteristics refer to the conditions at the start of data collection of each experiment.

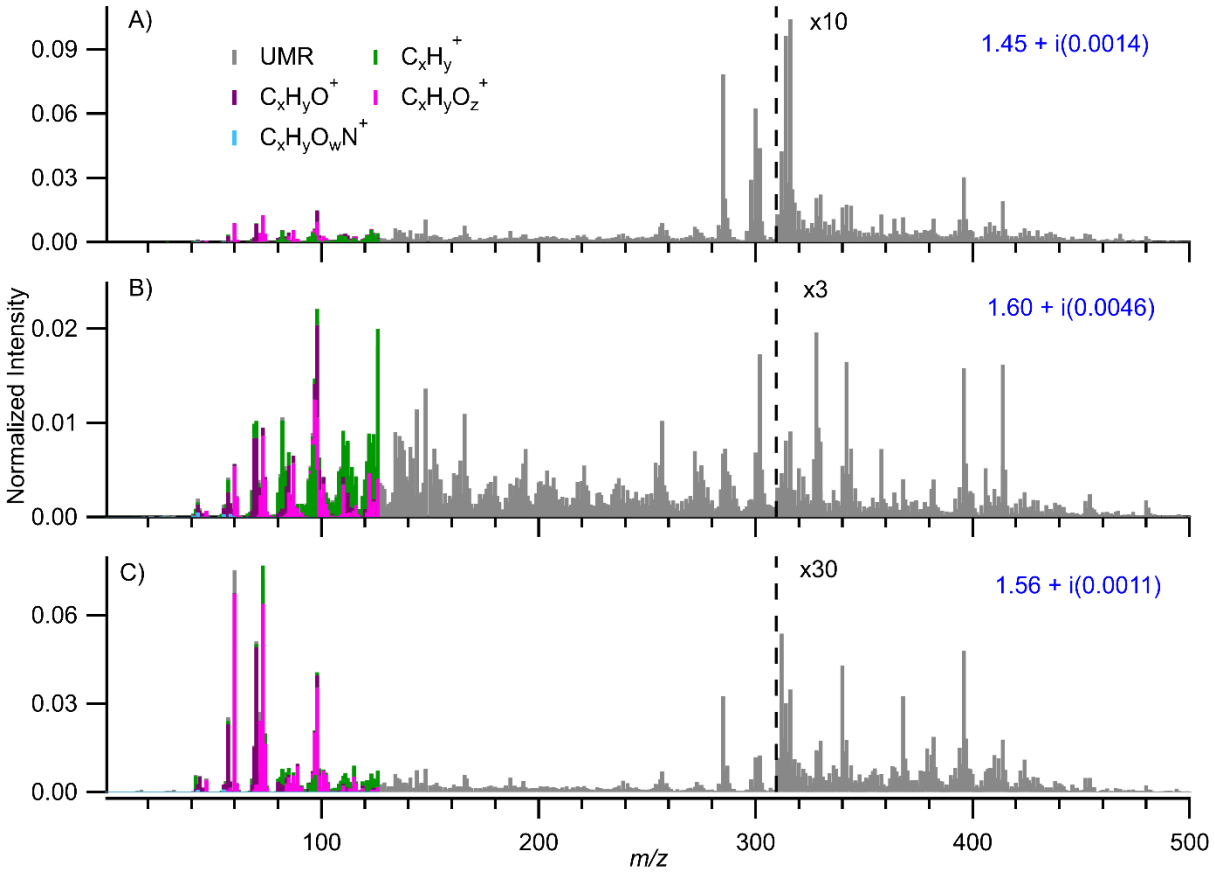

Figure S1 Chemical composition at the beginning of a smoldering event for three different sets of pine needles showing variation between samples. The complex index at 405 nm is shown in blue text for each sample. The use of vacuum ultraviolet (VUV) ionization for these samples allows for increased molecular information beyond what is achievable with standard (electron ionization; EI) AMS. As such, the apparent variation in chemical composition is much larger than what would be observed with EI-AMS.

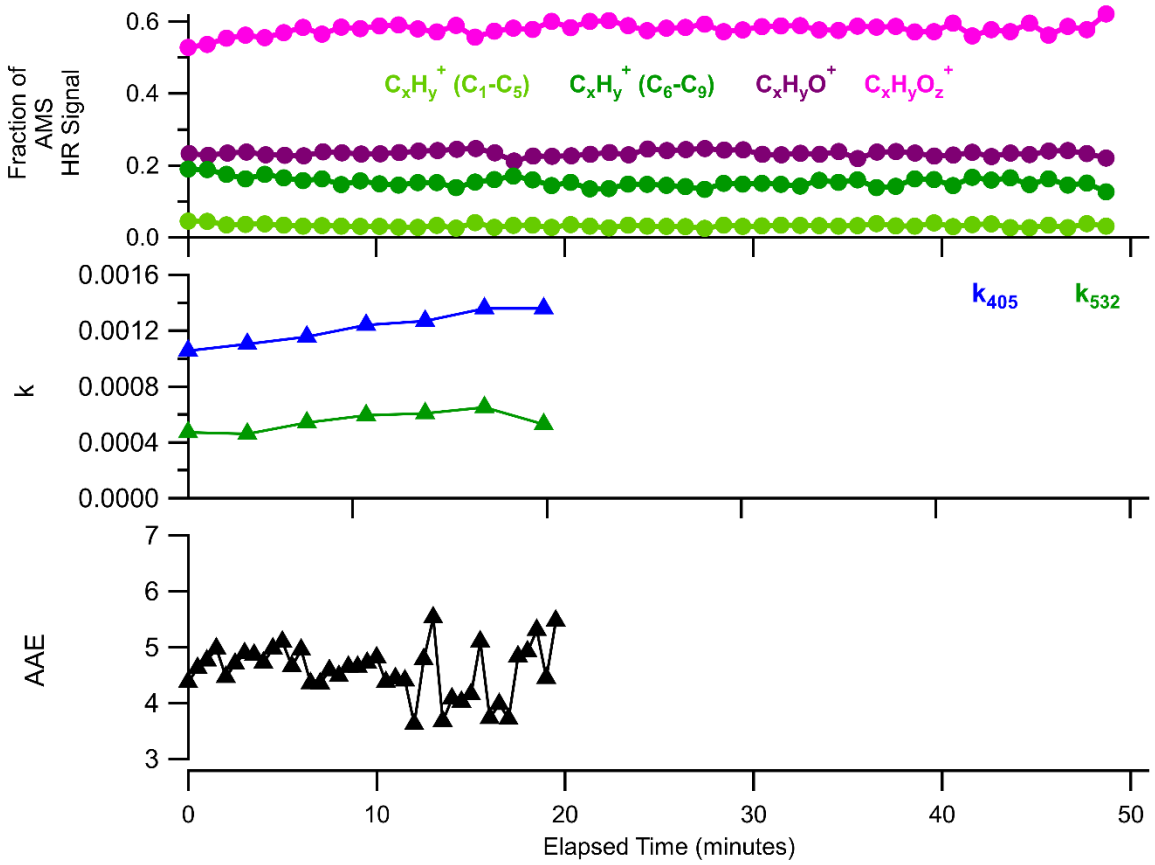

Figure S2 Evolution of the composition and optical properties of unoxidized aerosol over the course of a smoldering event. Due to decreasing aerosol concentration, the optical measurements are not reported after ~20 minutes. Substantially less within sample variability is observed when compared to between sample variability (Fig. S1). Although changes occur within the first ~10 minutes, the changes per unit time are small compared to the oxidative changes described in the main text.

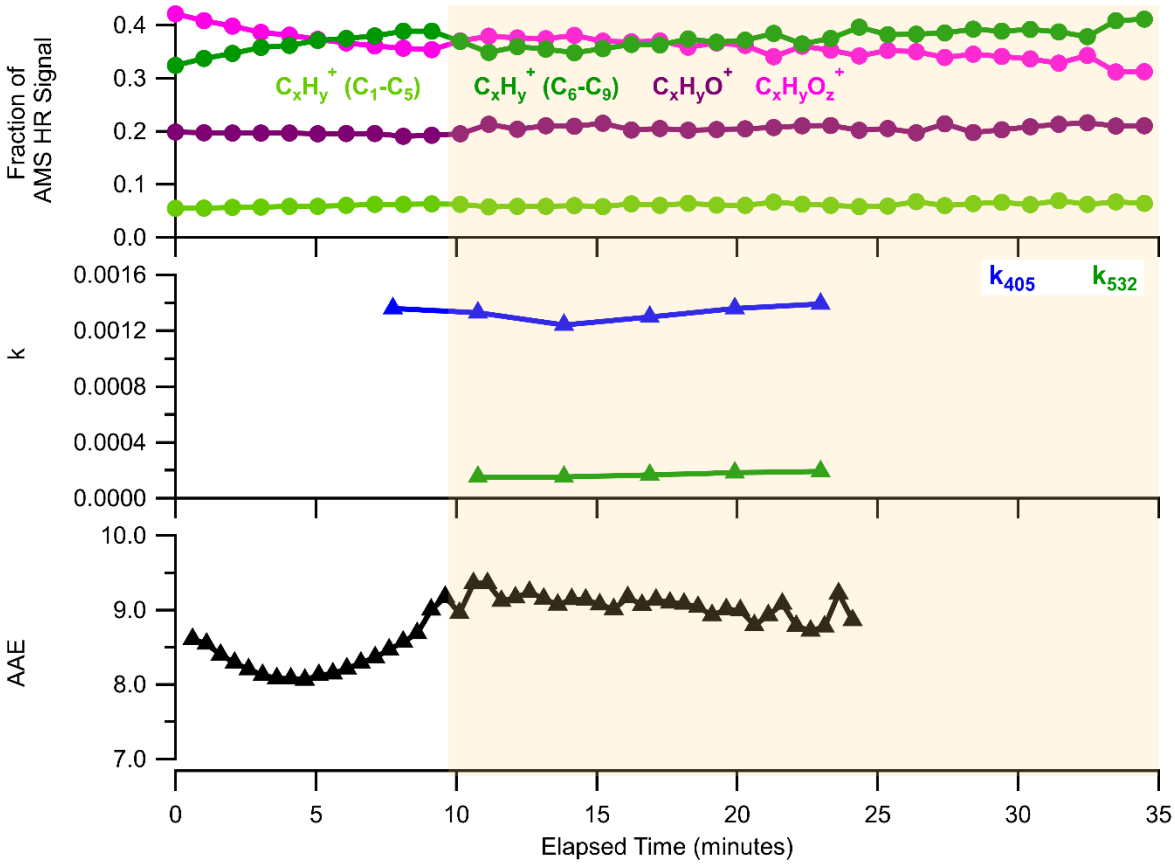

Figure S3 Example of the effect of 254 nm lights on the evolution of the composition and optical properties of unoxidized aerosol over the course of a smoldering event. Extinction data was unavailable at the beginning of the measurement period and thus refractive indices are not retrieved for that time period. At ~10 minutes after the start of this event, the 254 nm lights are turned on (yellow shaded region). At this point the C_6-C_9 $C_xH_y^+$ ions slightly decrease, the $C_xH_yO_z^+$ ions slightly increase, and k_{405} slightly decreases. These changes may be the result of either photolysis or the increased temperature of the flow tube from the presence of the lights altering the composition and optical properties of the aerosol. Given that the residence time of the aerosols in the flow tube remains constant in all the experiments, bleaching/composition changes are expected to be a constant effect in a given smoldering experiment and thus will not affect the interpretation of the oxidation results.

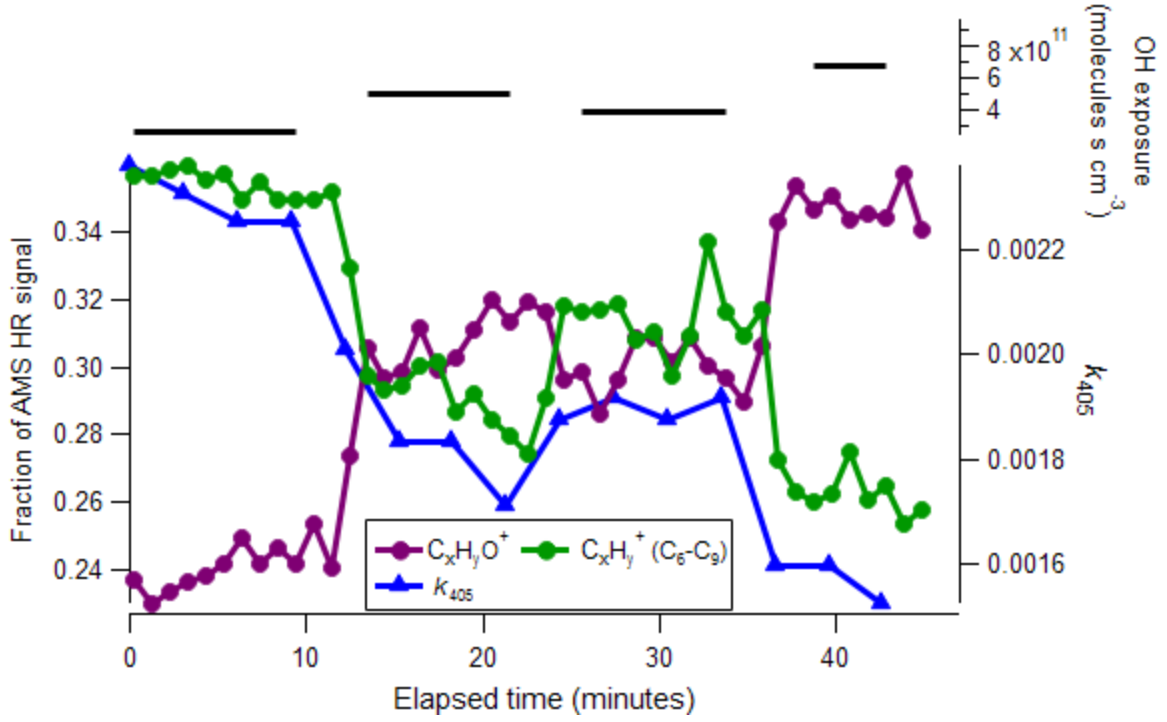

Figure S4 Raw data showing changes in composition and k_{405} during the OH + ozone experiments. OH exposure is altered in a non-monotonic fashion. The observed changes indicate that the decrease in k_{405} with increased OH exposure results from oxidation and not from long-term drift. Symbols indicate the midpoint of the measurement time.

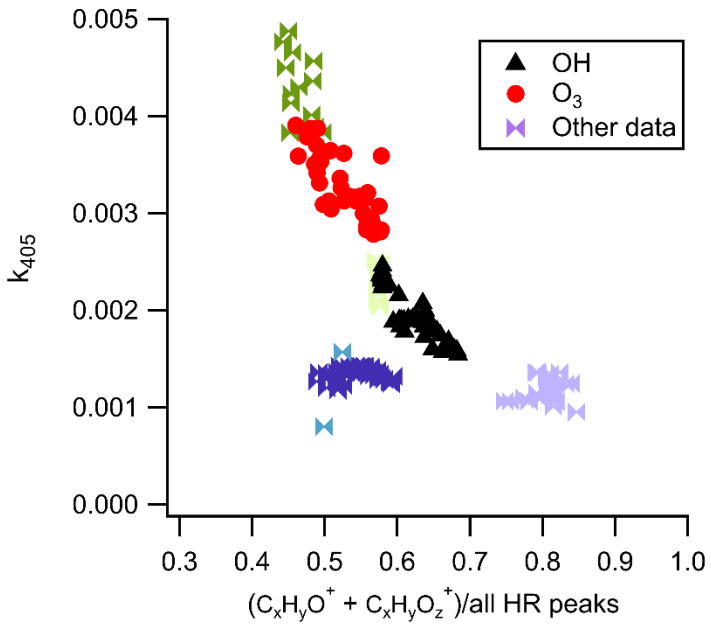

Figure S5 Relationship between k_{405} and the aerosol oxygen content. The heterogeneous oxidation data discussed in the main text is included (same as Fig. 4). The points labeled "other data" are results from smoldering events where no oxidation occurred (Figs. S2-S3) and events where heterogeneous oxidation occurred but insufficient data was collected to perform a kinetic analysis. Each smoldering event is represented by a different color. Measurements during transitions between oxidant levels in the flow tube are included unlike in the kinetic analysis. Although several of the events appear to follow a similar trend, two events where about half the ions contained oxygen exhibit significantly lower absorption than the other samples. Thus, while ensemble measurements of composition may be useful in understanding the decrease in absorption with increased oxidation for a given sample, these measurements cannot be used to predict absorption when multiple samples are considered.

References

Chakrabarty, R.K., H. Moosmüller, L.-W.A. Chen, K. Lewis, W.P. Arnott, C. Mazzoleni, M.K. Dubey, C.E. Wold, W.M. Hao, and S.M. Kreidenweis. 2010. Brown Carbon in Tar Balls from Smoldering Biomass Combustion. *Atmos. Chem. Phys.* 10 (13): 6363–6370. doi:10.5194/acp-10-6363-2010.

Martins, J.V., P.V. Hobbs, R.E. Weiss, and P. Artaxo. 1998. Sphericity and Morphology of Smoke Particles from Biomass Burning in Brazil. *Journal of Geophysical Research: Atmospheres* 103 (D24): 32051–32057. doi:10.1029/98JD01153.

Pósfai, M., A. Gelencsér, R. Simonics, K. Arató, J. Li, P.V. Hobbs, and P.R. Buseck. 2004. Atmospheric Tar Balls: Particles from Biomass and Biofuel Burning. *Journal of Geophysical Research: Atmospheres* 109 (D6). doi:10.1029/2003JD004169.

Sumlin, B.J., A. Pandey, M.J. Walker, R.S. Pattison, B.J. Williams, and R.K. Chakrabarty. 2017. Atmospheric Photooxidation Diminishes Light Absorption by Primary Brown Carbon Aerosol from Biomass Burning. *Environmental Science & Technology Letters* 4 (12): 540–545. doi:10.1021/acs.estlett.7b00393.

Zarzana, K.J., C.D. Cappa, and M.A. Tolbert. 2014. Sensitivity of Aerosol Refractive Index Retrievals Using Optical Spectroscopy. *Aerosol Science and Technology* 48 (11): 1133–1144. doi:10.1080/02786826.2014.963498.